ACADEMIC PRESS

Available online at www.sciencedirect.com

SCIENCE DIRECT®

Journal of Sound and Vibration 263 (2003) 965–977

JOURNAL OF SOUND AND VIBRATION

www.elsevier.com/locate/jsvi

Vibrations of oblique shear-deformable plates

R. Heuer*, F. Ziegler

Department of Civil Engineering, Vienna University of Technology, Wiedner Hauptstr. 8-10/E201, A-1040 Vienna, Austria

Accepted 4 February 2003

Abstract

The proposed numerical analysis of moderately thick plates subject to rather general boundary conditions is based on the direct boundary element method (BEM) in the frequency domain. First order shear-deformation theory of the Reissner–Mindlin-type is considered. A step forward in efficiency is obtained when the force and double force with moment Green's functions of the rectangular simply supported base plate of the same stiffness are applied. The time-reduced equations of hard-hinged polygonal plates correspond to those of a background Kirchhoff plate having frequency-dependent effective parameters like mass, lateral and in-plane load, and is further forced by imposed fictitious curvatures. This analogy holds even for the quasi-static shear forces and bending moments, i.e., when inertia effects become negligible. Furthermore, it can be shown that, in the static case, these stress resultants for certain groups of Reissner-type shear-deformable plates are identical with those resulting from the Kirchhoff theory in the background. Since this analogy is restricted to hard-hinged supports of straight edges, it is necessary to apply, e.g., the direct BEM of analysis to the plate of general planform and boundary conditions. The main effort is thus to study the properties and effective representations of the Green's dyadics and their singularities, in view of their proper integration. Similarly as for Kirchhoff plates, the strong singularity of the infinite domain is identified for the rectangular plate and subject to indirect integration. The resulting direct BEM proves to be efficient, robust and, in connection with proper pre- and post-processors, becomes an effective tool of engineering analyses just within the frequency limits given by the first two of the three spectral branches.

1. Introduction

Vibration of plates and shells have become the main topics of the dynamics of continuous structures, and Leissa's comprehensive monographs [1,2] are recognized as the most informative

*Corresponding author. Tel.: +43-1-58801-20130; fax: +43-1-58801-20199.
E-mail address: rh@allmech9.tuwien.ac.at (R. Heuer).

0022-460X/03/$ - see front matter
doi:10.1016/S0022-460X(03)00268-2

and definitive works in this field. In addition to the analysis of plates of various geometry and boundary conditions according to the classical Lagrange–Kirchhoff thin-plate theory, refined plate theories taking into account the influence of shear, rotatory inertia, and transverse normal stress have been developed in the literature, see e.g., the references given in Ref. [3]. Since the complexity of the resulting equations is quite high, there was a need for benchmark solutions, suitable for calibration of numerical routines. Furthermore, the question, whether results of the thin-plate theory correspond directly to those of the refined theories, a challenging task of analysis with reference to the background concept, is investigated in Ref. [4].

In the present paper, a numerical direct boundary element method (BEM) of analysis of moderately thick plates subject to rather general boundary conditions is developed. Numerical efficiency is improved when the Green's function of the rectangular simply supported base plate of the same stiffness is applied. It has been shown in Ref. [4] that the time-reduced equations (i.e., in the frequency domain) of hard-hinged polygonal plates reduce to those of a lower order background, e.g., to a Kirchhoff plate having effective mass and being loaded by effective lateral and in-plane forces and by imposed fictitious "thermal-type" curvatures. The corresponding influence functions are derived by means of analogies between the refined problem and the classical theory. Using the direct BEM, free and forced vibrations of moderately thick transversely isotropic homogeneous plates are thus studied in the frequency domain, where the influences of plate shear and rotatory inertia (the latter will be neglected in the numerical study) are basically taken into account according to Mindlin's approximation [5]. Generalizing Mindlin's theory, the present formulation includes first order shear-deformation theories. The restriction to the first order theory presented in the paper is justified by the fact that, for a wide range of applications, first order shear-deformation theories provide a satisfactory compromise between accuracy and computational efficiency, see e.g. Ref. [6]. Also sandwich plates with thin faces, common structural elements in aeronautics, fit into the context of first order shear-deformation theories (see Refs. [7,8]). A survey of buckling and post-buckling behavior of laminated plates is given in Ref. [9].

Refined expressions for bending moments and shear forces have been studied in analogy to their thin-plate counterparts. In the static case, these stress resultants for certain groups of the Reissner-type shear-deformable plates become identical with those resulting from the Kirchhoff theory. The first account of this analogy has been presented in Ref. [10], where deflections as well as stress resultants have been discussed according to various static shear-deformable theories. Analogies concerning the natural frequencies of Reissner–Mindlin plates have been considered in Ref. [11], where various complicating effects have been taken into account, such as isotropic in-plane forces and a two-parameter foundation of the moderately thick plate. These analogies refer to the simpler cases of Kirchhoff plates as well as to vibrating pre-stressed membranes. The main result of the membrane analogy is that the flexural, thickness-shear, and thickness-twist modal frequencies of polygonal simply supported Reissner–Mindlin plates can be derived from Helmholtz equations with appropriate boundary conditions. An extension in the frequency domain, to include forced vibrations, has been given in Refs. [12,13], and similar analogies for laminated plates have been presented in Ref. [14].

2. Hard-hinged supported polygonal plates of the Reissner–Mindlin-type

In Ref. [5], Mindlin derived the sixth order system of differential equations for the deflection w and the cross-sectional rotations ψ_x, ψ_y, which, when properly generalized, takes the form

$$\frac{K}{2}[(1-\nu)\Delta\psi_x + (1+\nu)(\psi_{x,x}+\psi_{y,y})_{,x}] - \frac{1}{s}(\psi_x + w_{,x}) = r\ddot{\psi}_x, \tag{1}$$

$$\frac{K}{2}[(1-\nu)\Delta\psi_y + (1+\nu)(\psi_{x,x}+\psi_{y,y})_{,y}] - \frac{1}{s}(\psi_y + w_{,y}) = r\ddot{\psi}_y, \tag{2}$$

$$\frac{1}{s}(\Delta w + \psi_{x,x} + \psi_{y,y}) + p = \rho h\ \ddot{w}, \tag{3}$$

$$K = Eh^3/12(1-\nu^2), \quad s = 1/\kappa^2 G^* h, \quad r = \rho h^3/12. \tag{4}$$

In Eqs. (1)–(4), (x, y) denote a global Cartesian co-ordinate system, and Δ is the two-dimensional Laplace operator. Several tracers are used in Eqs. (1)–(3) to account for various effects; s denotes a shear tracer, and G^* takes into account the effect of transverse isotropy. If $G^* = G$, i.e., G^* is equal the shear modulus G, the material is isotropic. The moderately large but constant thickness of the homogeneous plate is denoted h, and ρ is the mass density. Pao and Kaul [15] reported about the proper choice of the shear factor κ^2. The terms on the right-hand sides of Eqs. (1)–(3) are due to rotatory and transverse inertia, respectively, where a dot denotes the time differentiation, and r accounts for the influence of rotatory inertia, Eq. (4).

In the frequency domain, elimination of the cross-sectional rotations by adding properly differentiated Eqs. (1) and (2) and substituting $(\psi_{x,x} + \psi_{y,y})$ from Eq. (3), render the fourth order equation of an effectively loaded Kirchhoff plate in the frequency domain, hence defining a lower order background structure,

$$\Omega: \quad K\Delta\Delta w - \bar{n}\Delta w - \bar{\mu}w = \bar{q} - \Delta\bar{M}^{\mathrm{T}}, \tag{5}$$

where the time factor $\exp(\mathrm{i}\omega t)$ is understood, and the effective (frequency-dependent) parameters are

$$\bar{n} = -(Ks\rho h + r)\omega^2, \quad \bar{\mu} = \rho h\omega^2(1 - rs\omega^2), \quad \bar{q} = p(1 - rs\omega^2), \quad \bar{M}^{\mathrm{T}} = Ksp. \tag{6}$$

$\bar{n}$ and $\bar{\mu}$ denote effective hydrostatic in-plane force and mass density of unit plate area, respectively, and $\bar{q}$ is an effective transverse force loading. p is the actual lateral time harmonic pressure load and $\bar{M}^{\mathrm{T}}$ is a fictitious curvature (see Ref. [16] for governing equations of actually thermally loaded plates).

Any solution of Eq. (5) is a particular solution for the deflection of the Reissner–Mindlin problem, governed by Eqs. (1)–(4) with assigned frequency. It is shown in Ref. [4] that the analogy is complete for polygonal-shaped plates with hard-hinged supports. The boundary conditions of this simply supported Reissner–Mindlin plate, where (n, s) denotes a local Cartesian co-ordinate system at the boundary Γ with the unit normal $\mathbf{n}$,

$$\Gamma: \quad w = 0, \quad \psi_s = 0, \quad m_n = K(\psi_{n,n} + \nu\psi_{s,s}) = 0, \tag{7}$$

are transformed to a simpler form in the special case of straight edge segments, by noting from the second condition in Eq. (7) that $\psi_{s,s} = 0$ along the boundary Γ. Therefore, the third boundary

condition (7) reduces to $\psi_{n,n} = 0$. Substitution into Eq. (3), which is considered to hold along the straight edge segment, results in the non-homogeneous Navier boundary conditions

$$\Gamma: \quad w = 0, \quad K\Delta w = -\bar{M}^{\mathrm{T}}. \tag{8}$$

Eqs. (5) and (8) correspond to the boundary value problem of a simply supported Kirchhoff plate with an effective load $\bar{q}$ and an imposed curvature-type load $\bar{M}^{\mathrm{T}}$. In the special case of hard-hinged boundary conditions, no singular supporting forces appear at the corner points of the boundary Γ.

3. The shear-deformable plate with force and moment load

Subsequently, the original Mindlin plate theory is simplified by neglecting the rotatory inertia so that $r = 0$. Hard-hinged boundary conditions understood, the modified relations given subsequently thus remain exactly valid in the static problem, $\omega \to 0$, and, e.g., remains approximately valid for dynamically loaded plates made of transversely isotropic material, where the ratio $E/G^* \gg 2(1+\nu)$, where E denotes the in-plane elastic modulus. In this case, it can be expected that the effect of shear deformation dominates over the effect of rotatory inertia. Including the additional action of distributed moment loads $\bar{m}_x$ and $\bar{m}_y$ (especially in view of the determination of the Green's dyadics), the following modified boundary value problem is obtained (see also Ref. [17]):

$$\Omega: \quad K\Delta\Delta w - \bar{n}\Delta w - \bar{\mu} w = p - Ks\Delta p + K\Delta V, \tag{9}$$

$$\Gamma: \quad w = 0, \quad \Delta w = V - sp, \tag{10}$$

where, observing simplifications in Eq. (6) and the additional term for the distributed moment load,

$$\bar{n} = -Ks\rho h\omega^2, \quad \bar{\mu} = \rho h\,\omega^2, \quad V_{,i} = \bar{m}_i/K, \quad i = x, y. \tag{11}$$

The cross-sectional rotations then become, with the deflection due to force and moment load substituted and rotatory inertia neglected (see also Ref. [4] for detailed derivation)

$$\psi_i = -Ks[\Delta w + s(p + \rho h\,\omega^2 w) - V]_{,i} - w_{,i}, \quad i = x, y. \tag{12}$$

Both the bending moments and the shear forces in the Mindlin plate are given by the constitutive law for the linear elastic plate,

$$\begin{bmatrix} m_x \\ m_y \\ m_{xy} \end{bmatrix} = K \begin{bmatrix} 1 & \nu & 0 \\ \nu & 1 & 0 \\ 0 & 0 & (1-\nu)/2 \end{bmatrix} \begin{bmatrix} \psi_{x,x} \\ \psi_{y,y} \\ \psi_{x,y} + \psi_{y,x} \end{bmatrix}, \tag{13}$$

$$q_i = \frac{1}{s}(\psi_i + w_{,i}) = -K[\Delta w + s(p + \rho h\omega^2 w) - V]_{,i}, \quad i = x, y. \tag{14}$$

4. Influence functions of hard-hinged supported rectangular shear-deformable homogeneous plates

The Green's dyadics for the single force and the double force with moment of a rectangular plate (a,b), are subsequently derived by differentiating properly the force deflection Green's function and by employing the analogy to the effective Kirchhoff background.

4.1. The force influence functions

The lateral deflection of the rectangular plate at the point $\boldsymbol{\xi} = (\xi,\eta)^{\mathrm{T}}$ due to a unit single force acting at the source point $\mathbf{x} = (x,y)^{\mathrm{T}}$, $p = \delta(\mathbf{x}-\boldsymbol{\xi})$, can be expressed in the form of a double series (see, e.g., Ref. [18]):

$$\tilde{w}(\boldsymbol{\xi},\mathbf{x};\lambda) = \frac{4}{abK}\sum_{m=1}^{\infty}\sum_{n=1}^{\infty}\frac{(1+Ks\ \alpha_{mn})\sin\frac{m\pi\xi}{a}\sin\frac{n\pi\eta}{b}\sin\frac{m\pi x}{a}\sin\frac{n\pi y}{b}}{[\alpha_{mn}^2-\lambda^4(1+Ks\alpha_{mn})]}, \tag{15}$$

where

$$\lambda^4 = \frac{\rho h\omega^2}{K}, \quad \alpha_{mn} = \left[\left(\frac{m\pi}{a}\right)^2+\left(\frac{n\pi}{b}\right)^2\right]. \tag{16}$$

The result can be verified by applying the analogy (i.e., by considering the single-force loaded rectangular effective Kirchhoff background plate), thus solving Eq. (9) with $V=0$. Due to the shear influence, this solution exhibits the weak singularity, $\sim \ln r$, where $r = |\mathbf{x}-\boldsymbol{\xi}| \to 0$.

The reduction to a fast-convergent single-sum representation has been derived in Ref. [12], that is given by

$$\tilde{w}(\boldsymbol{\xi},\mathbf{x},\lambda) = \sum_{m=1}^{\infty}(a_m^{(1)}+a_m^{(2)})\sin\frac{m\pi x}{a}, \tag{17}$$

with the following abbreviations:

$$\begin{aligned}
a_m^{(j)}(\lambda;y) &= \frac{(-1)^j}{aK}\frac{(1+Ks\ \alpha_j)}{\Delta(\lambda)}\frac{\sin\frac{m\pi\xi}{a}}{k_m^{(j)}[1-\exp(-2k_m^{(j)}b)]}(E_m^{(j)}+F_m^{(j)}),\\
E_m^{(j)}(\eta,y;k_m^{(j)}) &= \exp[-k_m^{(j)}|y-\eta|]-\exp[-k_m^{(j)}(y+\eta)],\\
F_m^{(j)}(\eta,y;b,k_m^{(j)}) &= \exp[-k_m^{(j)}(2b-|y-\eta|)]-\exp[-k_m^{(j)}(2b-|y+\eta|)],\\
k_m^{(j)} &= \sqrt{(m\pi/a)^2-\alpha_j}, \quad \alpha_{1,2} = \frac{1}{2}[Ks\lambda^4 \pm \sqrt{(Ks\lambda^4)^2+4\lambda^4}], \qquad j=1,2.
\end{aligned} \tag{18}$$

The cross-sectional rotation for the case of the force load is calculated in terms of derivatives of the deflection w and the unit single force, according to Eq. (12), and again setting $V\equiv 0$,

$$\tilde{\psi}_i = -\frac{4}{abK}\sum_{m=1}^{\infty}\sum_{n=1}^{\infty}\frac{[\sin\frac{m\pi\xi}{a}\sin\frac{n\pi\eta}{b}\sin\frac{m\pi x}{a}\sin\frac{n\pi y}{b}]_{,i}}{[\alpha_{mn}^2-\lambda^4(1+Ks\alpha_{mn})]}, \quad i = n(\boldsymbol{\xi}), s(\boldsymbol{\xi}), \tag{19}$$

$$(.)_{,n} = \frac{\partial}{\partial n(\boldsymbol{\xi})}(.) = (.)_{,\xi}n_\xi + (.)_{,\eta}n_\eta, \quad (.)_{,s} = \frac{\partial}{\partial s(\boldsymbol{\xi})}(.) = (.)_{,\xi}s_\xi + (.)_{,\eta}s_\eta. \tag{20}$$

The force influence functions of the cross-sectional rotations $\tilde{\psi}_i$ show a regular behavior in the limit $r = |\mathbf{x} - \boldsymbol{\xi}| \to 0$, and (n, s) denotes a local orthogonal co-ordinate system at the observation point $\boldsymbol{\xi}$.

The force influence bending moments are derived by inserting the derivatives of Eq. (19) into Eq. (13), exhibiting the same weak singularity $\sim \ln r$, where $r = |\mathbf{x} - \boldsymbol{\xi}| \to 0$ as observed in the case of the deflection, represented by Eq. (15).

The force influence shear forces, however, are strongly singular of the order one, $\sim r^{-1}$ where $r = |\mathbf{x} - \boldsymbol{\xi}| \to 0$,

$$\tilde{q}_i(\boldsymbol{\xi}, \mathbf{x}; \lambda) = \sum_{m=1}^{\infty} \sum_{n=1}^{\infty} (c_{mn}^{(1)} + c_{mn}^{(2)})_{,i} \sin \frac{m\pi x}{a} \sin \frac{n\pi y}{b}, \quad i = n(\boldsymbol{\xi}), s(\boldsymbol{\xi}), \tag{21}$$

$$c_{mn}^{(j)}(\lambda) = \frac{4(-1)^j}{abK} \frac{\alpha_{mn}}{\Delta(\lambda)} \frac{\sin \frac{m\pi\xi}{a} \sin \frac{n\pi\eta}{b}}{(\alpha_j - \alpha_{mn})}, \quad \Delta(\lambda) = \sqrt{(Ks\lambda^4)^2 + 4\lambda^4}, \qquad j = 1, 2. \tag{22}$$

4.2. The moment influence functions

The moment influence function of the shear-deformable rectangular plate is considered by taking into account a double force (parallel to the midplane) with a time harmonic moment per unit of area. Applying the analogy to the effective background Kirchhoff plate, Eqs. (9) and (10) are to be solved, setting $p \equiv 0$ and considering $V_{,m} = K^{-1}\delta(\mathbf{x} - \boldsymbol{\xi})$, where m gives the direction in the midplane with respect to the Cartesian co-ordinates, see Eq. (11). The right-hand side of Eq. (9) is thus proportional to the derivative of the concentrated moment. Inspecting the deflections resulting from the force and moment load, we note that the latter is given by proper differentiation of the force influence function in Eq. (15),

$$\tilde{w}^{M_k}(\mathbf{x}, \boldsymbol{\xi}; \lambda) = \frac{\partial}{\partial k(\mathbf{x})} \left(\frac{4}{abK} \sum_{m=1}^{\infty} \sum_{n=1}^{\infty} \frac{\sin \frac{m\pi\xi}{a} \sin \frac{n\pi\eta}{b} \sin \frac{m\pi x}{a} \sin \frac{n\pi y}{b}}{[\alpha_{mn}^2 - \lambda^4(1 + Ks\alpha_{mn})]} \right), \quad k = n(\mathbf{x}), s(\mathbf{x}), \tag{23}$$

where the shear factor in the nominator must be put to zero, and, as is known from the classical solution of the Kirchhoff plate by taking the derivative with respect to the point of application of the concentrated moment $\mathbf{x}$ (compare, e.g., Ref. [19]),

$$(.)_{,n} = \frac{\partial}{\partial n(\mathbf{x})}(.) = (.)_{,x} n_x + (.)_{,y} n_y, \quad (.)_{,s} = \frac{\partial}{\partial s(\mathbf{x})}(.) = (.)_{,x} s_x + (.)_{,y} s_y. \tag{24}$$

The moment influence function exhibits a regular behavior in the limit $r = |\mathbf{x} - \boldsymbol{\xi}| \to 0$.

When calculating the influence functions of the cross-sectional rotations, $p \equiv 0$ in Eq. (12), by substituting the moment influence deflection of Eq. (23), an additional, shear-determined dynamical term enters with the result of the appearance of a weak singularity, $\sim \ln r$, where $r = |\mathbf{x} - \boldsymbol{\xi}| \to 0$. (see Ref. [17] for detailed derivation),

$$\tilde{\psi}_i^{M_k}(\boldsymbol{\xi}, \mathbf{x}; \lambda) = \frac{4}{abK} \sum_{m=1}^{\infty} \sum_{n=1}^{\infty} \Psi_{mn} \left(\sin \frac{m\pi\xi}{a} \sin \frac{n\pi\eta}{b} \right)_{,i(\xi)} \left(\sin \frac{m\pi x}{a} \sin \frac{n\pi y}{b} \right)_{,k(x)}, \tag{25}$$

$$\Psi_{mn} = [Ks\alpha_{mn} - (Ks)^2\lambda^4 - 1][\alpha_{mn}^2 - \lambda^4(1 + Ks\alpha_{mn})]^{-1}. \tag{26}$$

The moment-determined moment influence functions are derived from Eq. (13) by substituting the derivatives of Eq. (25). As expected, a first order strong singularity is encountered, $\sim r^{-1}$, where $r = |\mathbf{x} - \boldsymbol{\xi}| \to 0$.

The moment influence functions of the shear forces exhibiting the weak singularity $\sim \ln r$, where $r = |\mathbf{x} - \boldsymbol{\xi}| \to 0$, are explicitly derived by setting $p \equiv 0$ in the more cumbersome expression given by Eq. (14):

$$\tilde{q}_i^{M_k}(\boldsymbol{\xi}, \mathbf{x}; \lambda) = \frac{4}{ab} \sum_{m=1}^{\infty} \sum_{n=1}^{\infty} Q_{mn} \left(\sin \frac{m\pi\xi}{a} \sin \frac{n\pi\eta}{b} \right)_{,i(\xi)} \left(\sin \frac{m\pi x}{a} \sin \frac{n\pi y}{b} \right)_{,k(x)}, \tag{27}$$

$$Q_{mn} = [\alpha_{mn} - Ks\lambda^4 - 1][\alpha_{mn}^2 - \lambda^4(1 + Ks\alpha_{mn})]^{-1}, \quad \sim \ln r, \quad r = |\mathbf{x} - \boldsymbol{\xi}| \to 0. \tag{28}$$

5. Direct BEM for shear-deformable plates with classical boundary conditions under lateral force loading

The differential equation (9) is applied without considering the moment per unit of area, thus $V \equiv 0$. It is solved subsequently, after transforming it into an integral equation, where the state vector is given by (see, e.g., Ref. [20])

$$\begin{bmatrix} w(\mathbf{x}) \\ \psi_n(\mathbf{x}) \\ \psi_s(\mathbf{x}) \end{bmatrix} + \int_\Gamma \begin{bmatrix} \tilde{q}_n & \tilde{m}_n & \tilde{m}_{ns} \\ \tilde{q}_n^{M_n} & \tilde{m}_n^{M_n} & \tilde{m}_{ns}^{M_n} \\ \tilde{q}_n^{M_s} & \tilde{m}_n^{M_s} & \tilde{m}_{ns}^{M_s} \end{bmatrix} \begin{bmatrix} w \\ \psi_n \\ \psi_s \end{bmatrix} \mathrm{d}\Gamma$$
$$= \int_\Gamma \begin{bmatrix} \tilde{w} & \tilde{\psi}_n & \tilde{\psi}_s \\ \tilde{w}^{M_n} & \tilde{\psi}_n^{M_n} & \tilde{\psi}_s^{M_n} \\ \tilde{w}^{M_s} & \tilde{\psi}_n^{M_s} & \tilde{\psi}_s^{M_s} \end{bmatrix} \begin{bmatrix} q_n \\ m_n \\ m_{ns} \end{bmatrix} \mathrm{d}\Gamma + \int_\Omega \begin{bmatrix} \tilde{w}p \\ 0 \\ 0 \end{bmatrix} \mathrm{d}\Omega. \tag{29}$$

The direct BEM is then applied by considering boundary conditions given in Table 1.

Discretizing the actual boundary of the Mindlin plate according to the collocation method and by considering Eq. (29) at the boundary, $\mathbf{x} \to \mathbf{s}$, gives, using hypermatrix notation,

$$\mathbf{Hu} = \mathbf{Lf} + \mathbf{p}, \tag{30}$$

where $\mathbf{u}$ contains the kinematic values at the collocation points, $\mathbf{f}$ represents the dynamic boundary conditions at these points, and $\mathbf{p}$ is the particular deflection integral due to the external lateral load p.

Table 1
Classical boundary conditions of the shear-deformable plate

Hard-hinged support	$w = 0$	$m_n = 0$	$\psi_s = 0$
Soft-hinged support	$w = 0$	$m_n = 0$	$m_{ns} = 0$
Clamped	$w = 0$	$\psi_n = 0$	$\psi_s = 0$
Free	$m_n = 0$	$q_n = 0$	$m_{ns} = 0$

All elements of matrix $\mathbf{L}$, the submatrices $\mathbf{H}_2$, $\mathbf{H}_3$, $\mathbf{H}_1^{M_n}$, $\mathbf{H}_1^{M_s}$ of the hypermatrix

$$\mathbf{H} = \begin{bmatrix} \mathbf{H}_1 & \mathbf{H}_2 & \mathbf{H}_3 \\ \mathbf{H}_1^{M_n} & \mathbf{H}_2^{M_n} & \mathbf{H}_3^{M_n} \\ \mathbf{H}_1^{M_s} & \mathbf{H}_2^{M_s} & \mathbf{H}_3^{M_s} \end{bmatrix}, \tag{31}$$

and all the remaining off-diagonal elements of $\mathbf{H}$ contain regular or weakly singular integrals. The regular integrals are evaluated numerically by means of the standard Gaussian quadrature formula. The weakly singular integrals are determined by splitting the corresponding influence function into the singular (logarithmic) part of the infinite plate domain and a remaining regular part, that accounts for the hard-hinged boundary conditions, compare Ref. [13]. The latter is again evaluated by means of the standard Gaussian quadrature formula. The weakly singular part is computed by using the one-dimensional logarithmic Gaussian integration scheme, see, e.g., Ref. [21].

The diagonal elements of $\mathbf{H}_1$, $\mathbf{H}_2^{M_n}$, $\mathbf{H}_3^{M_n}$, $\mathbf{H}_2^{M_s}$, $\mathbf{H}_3^{M_s}$, exhibit strong singularities and therefore they are considered separately. Strongly singular integrals of the first kind are integrated indirectly by applying the following rigid body motions of the actual plate (see Ref. [22] for details):

(i) a unit translation in the lateral direction:

$$\begin{bmatrix} \mathbf{H}_1 & \mathbf{H}_2 & \mathbf{H}_3 \\ \mathbf{H}_1^{M_n} & \mathbf{H}_2^{M_n} & \mathbf{H}_3^{M_n} \\ \mathbf{H}_1^{M_s} & \mathbf{H}_2^{M_s} & \mathbf{H}_3^{M_s} \end{bmatrix} \begin{bmatrix} \mathbf{I} \\ \mathbf{0} \\ \mathbf{0} \end{bmatrix} = \begin{bmatrix} \mathbf{0} \\ \mathbf{0} \\ \mathbf{0} \end{bmatrix} \Rightarrow H_{1ii} = -\sum_{\substack{j=1 \\ j \neq i}}^{K} H_{1ij}, \tag{32}$$

where j is the number of the collocation point, $j = 1, 2, \ldots, K$.

(ii) small unit rotations about the local (n, s) axes, respectively:

Note the projections of the radial distance on the co-ordinate axes, when inspecting Eqs. (33) and (34),

$$\begin{bmatrix} \mathbf{H}_1 & \mathbf{H}_2 & \mathbf{H}_3 \\ \mathbf{H}_1^{M_n} & \mathbf{H}_2^{M_n} & \mathbf{H}_3^{M_n} \\ \mathbf{H}_1^{M_s} & \mathbf{H}_2^{M_s} & \mathbf{H}_3^{M_s} \end{bmatrix} \begin{bmatrix} (x-\xi)_j \\ \mathbf{I} \\ \mathbf{0} \end{bmatrix} = \begin{bmatrix} \mathbf{0} \\ \mathbf{0} \\ \mathbf{0} \end{bmatrix} \Rightarrow H_{2ii}^{M_n}, H_{2ii}^{M_s}, \tag{33}$$

$$\begin{bmatrix} \mathbf{H}_1 & \mathbf{H}_2 & \mathbf{H}_3 \\ \mathbf{H}_1^{M_n} & \mathbf{H}_2^{M_n} & \mathbf{H}_3^{M_n} \\ \mathbf{H}_1^{M_s} & \mathbf{H}_2^{M_s} & \mathbf{H}_3^{M_s} \end{bmatrix} \begin{bmatrix} (y-\eta)_j \\ \mathbf{0} \\ \mathbf{I} \end{bmatrix} = \begin{bmatrix} \mathbf{0} \\ \mathbf{0} \\ \mathbf{0} \end{bmatrix} \Rightarrow H_{3ii}^{M_n}, H_{3ii}^{M_s}. \tag{34}$$

Sorting for the unknown (non-prescribed) boundary values in Eq. (30) results in a linear system of equations for the unknown kinematic and/or dynamic boundary values of the actual plate,

$$\mathbf{A}\mathbf{y} = \mathbf{B}. \tag{35}$$

6. Frequency response function of hard-hinged trapezoidal plates

As an illustrative example the frequency response function (FRF), $w(\Omega)/h$, of a trapezoidal plate due to a spatial uniform (time-harmonic) pressure load p_0 is presented. The geometry chosen is $a_1/b = 1.9$, $\gamma = 45^\circ$, and the deflection is determined at the central point $D(0.4a_1, 0.5b)$. The aspect ratio of the basic rectangular domain is $a/b = 2.3$, as shown in Fig. 1.

Non-dimensional inputs are the frequency parameter $\Omega = \omega a\sqrt{\rho/G}$, the load factor $p_0^* = p_0 6(1-\nu)a^3/Gh^3 = 1.0$, and the thickness ratio $h/a = 0.15$. The Mindlin shear factor of $\kappa^2 = \pi^2/12$ (see, e.g., Ref. [5]), and Poisson's ratio of $\nu = 0.2$ are selected.

In Figs. 2 and 3, examples of the force influence functions $\tilde{\psi}_x(\xi; x = a/2, y = b/2)$ according to Eq. (19), and $\tilde{m}_x(\xi; x = a/2, y = b/2)$ determined by substituting differentiated Eq. (19) into Eq. (13), of the basic rectangular domain with the non-dimensional forcing frequency $\Omega = 2.5$ assigned are illustrated. Note the weak singularity apparent in Fig. 3 at the point of application of the unit force.

The numerical BEM procedure, Eq. (30) is applied to the trapezoidal plate, considering two different boundary conditions along the oblique edge, with hard-hinged conditions assumed at the remaining three edges. The actual trapezoidal domain is embedded into the basic hard-hinged supported rectangular plate thus achieving coincidence along three boundaries $(\overline{AB}, \overline{CD}, \overline{DA})$, see Fig. 1. It is sufficient to discretize the oblique edge $\overline{BC}$ into 15 quadratic boundary elements.

The first result of the numerical analysis is the FRF of the undamped oblique plate. Linear damping should be subsequently considered by applying the quadrature-type elastic–viscoelastic correspondence principle holding in the frequency domain. By choosing a one-parameter

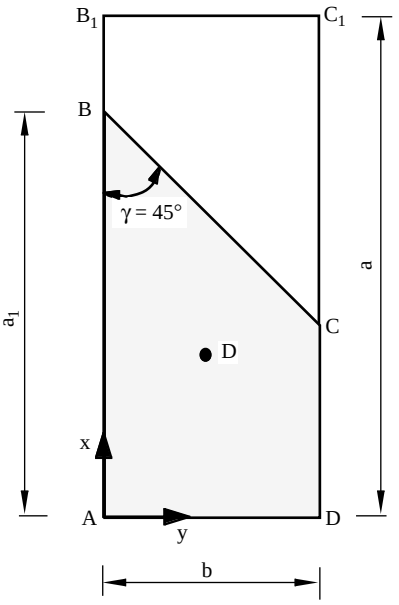

Fig. 1. Geometry of the trapezoidal plate embedded into a rectangular basic domain.

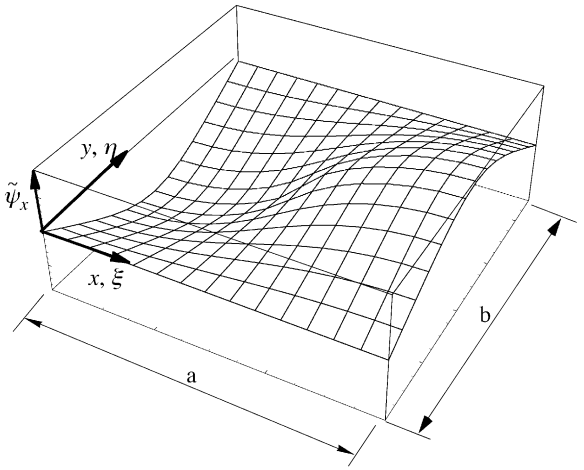

Fig. 2. Influence function of the cross-sectional rotation $\tilde{\psi}_x(\mathbf{x},\boldsymbol{\xi})$ due to a unit force acting at $\mathbf{x} = (a/2, b/2)^{\mathrm{T}}$; forcing frequency parameter $\Omega = \omega a\sqrt{\rho/G} = 2.5$.

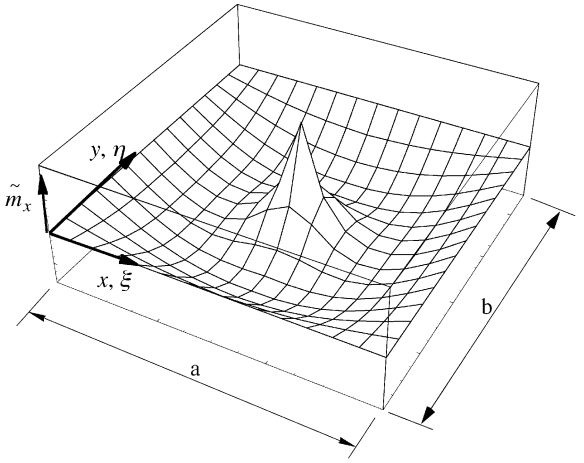

Fig. 3. Influence function of the bending moment $\tilde{m}_n(\mathbf{x},\boldsymbol{\xi})$ due to a unit force acting at $\mathbf{x} = (a/2, b/2)^{\mathrm{T}}$; forcing frequency parameter $\Omega = \omega a\sqrt{\rho/G} = 2.5$.

damping (e.g., a complex shear modulus) a simple integration of the weighted undamped FRF along the real frequency axis renders the damped FRF. For the description of this procedure, see Ref. [23].

6.1. Trapezoidal plate with clamped oblique edge

Inspection of Eq. (29) reveals the absence of strong singularities and the numerical evaluation of the matrix elements in $\mathbf{L}$ in Eq. (30) is reduced to the Gaussian integration scheme. As an

illustrative example the undamped FRF of deflection at the central point D (see Fig. 1) is shown in Fig. 4.

6.2. Hard-hinged supported trapezoidal plate

The numerical effort increases due to the appearance of strongly singular influence functions in the submatrices of **H**, as is seen by inspecting Eqs. (29) and (30). Thus, the indirect integration procedure, described in Eqs. (32)–(34), has to be applied in addition to the Gaussian integration scheme to obtain the coefficients in Eq. (30). The non-dimensional undamped FRF at the midpoint D (see Fig. 1) is shown in Fig. 5, exhibiting a lower number of resonances, when compared with Fig. 4 for the same frequency range.

Alternatively, in Ref. [13] the case of hard-hinged supported polygonal Mindlin plates is solved by considering Eqs. (9), (10) with $V \equiv 0$ and further splitting the effective Kirchhoff plate problem into two effective membrane problems of the same polygonal planform. Consequently, the indirect BEM is applied to the lower order Helmholtz problem for the membranes, thus circumventing the integration of strong singularities.

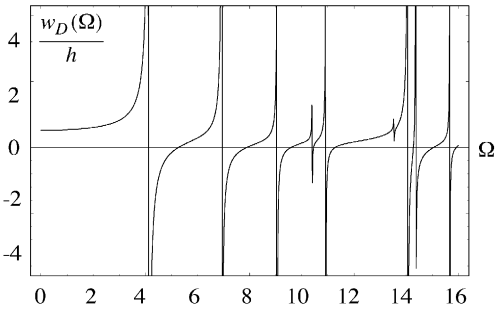

Fig. 4. Non-dimensional FRF $w_D(\Omega)/h$ at a central point $D(0.4a_1, 0.5b)$ due to $p_0^* = p_0 6(1-\nu)a^3/Gh^3 = 1.0$; frequency parameter $\Omega = \omega a\sqrt{\rho/G}$; hard-hinged supported along $(\overline{AB}, \overline{CD}, \overline{DA})$ and clamped along the skew edge $\overline{BC}$.

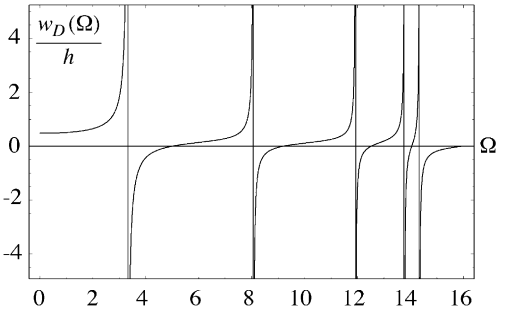

Fig. 5. Non-dimensional FRF $w_D(\Omega)/h$ at a central point $D(0.4a_1, 0.5b)$ due to $p_0^* = p_0 6(1-\nu)a^3/Gh^3 = 1.0$; frequency parameter $\Omega = \omega a\sqrt{\rho/G}$; hard-hinged supported along all edges.

7. Conclusions

The direct BEM is the most efficient numerical method available for the linear analysis of plates. Dynamically loaded shear-deformable plates are well characterized by frequency response functions. Consequently, the analysis is performed in the frequency domain. Plates of general planform are considered embedded in a rectangular and hard-hinged supported domain. For the latter, the force and double-force with moment Green's dyadics are derived by enforcing the analogy to a background Kirchhoff plate with frequency-dependent parameters. Some elements of the Green's dyadic exhibit strong singularities which are integrated indirectly by applying the kinematic approximation.

For the basic rectangular hard-hinged supported plate, relations to the Kirchhoff-plate background simplify the numerical analysis considerably with respect to the Green's dyadics.

A uniformly and time harmonically forced trapezoidal plate serves as illustration of the efficient numerical scheme, which is readily available for practical applications due to the listed Green's dyadics.

References

[1] A.W. Leissa, Vibration of plates, NASA SP-160, National Aeronautics and Space Administration, Washington, DC, 1969.
[2] A.W. Leissa, Vibration of shells, NASA SP-288, National Aeronautics and Space Administration, Washington, DC, 1973.
[3] E. Reissner, Reflections on the theory of elastic plates, Applied Mechanics Reviews 38 (1985) 1453–1464.
[4] H. Irschik, R. Heuer, F. Ziegler, Statics and dynamics of simply supported polygonal Reissner–Mindlin plates by analogy, Archive of Applied Mechanics 70 (2000) 231–244.
[5] R.D. Mindlin, Influence of rotatory inertia and shear on flexural motions of isotropic elastic plates, Journal of Applied Mechanics 18 (1951) 31–38.
[6] H. Irschik, F. Ziegler, Dynamics of composite structures based on lower order eigenstrains analysis, in: G.P. Cherepanov (Ed.), Fracture: A Topical Encyclopedia of Current Knowledge, Krieger, Malabar, 1998, pp. 840–852.
[7] K. Stamm, H. Witte, Sandwichkonstruktionen, Springer, Wien, 1974.
[8] L. Librescu, Elastostatics and Kinetics of Anisotropic and Heterogeneous Shell-type Structures, Noordhoff, Leyden, 1975.
[9] A.W. Leissa, Buckling and postbuckling theory for laminated composite plates, in: G.J. Turvey, I.J. Marshall (Eds.), Buckling and Postbuckling of Composite Plates, Chapman & Hall, London, 1995, pp. 3–29 (Chapter 1).
[10] H. Irschik, Eine Analogie zwischen Lösungen für schubstarre und schubelastische Platten, Zeitschrift für Angewandte Mathematik und Mechanik 62 (1982) T129–T131.
[11] H. Irschik, Membrane-type eigenmotions of Mindlin plates, Acta Mechanica 55 (1985) 1–20.
[12] R. Heuer, H. Irschik, A boundary element method for eigen-value problems of polygonal membranes and plates, Acta Mechanica 66 (1987) 9–20.
[13] H. Irschik, R. Heuer, F. Ziegler, Dynamic analysis of polygonal Mindlin plates on two-parameter foundation using classical plate theory and an advanced BEM, Computational Mechanics 4 (1989) 293–300.
[14] H. Irschik, On vibrations of layered beams und plates, Zeitschrift für Angewandte Mathematik und Mechanik 73 (1993) T34–T45.
[15] Y.-H. Pao, R.K. Kaul, Waves and vibrations in isotropic and anisotropic plates, in: G. Herrmann (Ed.), R.D. Mindlin and Applied Mechanics, Pergamon, New York, 1974, pp. 149–195.
[16] T.R. Tauchert, Thermally induced flexure, buckling and vibrations of plates, Applied Mechanics Reviews 44 (1991) 347–360.

[17] R. Heuer, F. Ziegler, BEM solutions of vibrating oblique moderately thick plates, in: V. Postnov (Ed.), Mathematical Modeling in Solid Mechanics, Boundary and Finite Element Methods, Proceedings of the 19th International Conference, Vol. III, Russia. Publ. St. Petersburg State University, St. Petersburg, 2001, pp. 169–188 (in Russian, translated by V. Postnov).
[18] E.B. Magrab, Vibrations of Elastic Structural Members, Sijthoff & Noordhoff, Alphen aan den Rijn, 1979.
[19] F. Hartmann, Introduction to Boundary Elements, Springer, Berlin, 1989.
[20] H. Antes, Static and dynamic analysis of Reissner–Mindlin plates, in: D.E. Beskos (Ed.), Boundary Element Analysis of Plates and Shells, Springer, Berlin, 1991, pp. 312–340.
[21] A.H. Stroud, D. Secrest, Gaussian Quadrature Formulas, Prentice-Hall, New York, 1966.
[22] F. Van der Weeën, Application of the boundary integral equation method to Reissner's plate model, International Journal of Numerical Methods in Engineering 18 (1982) 1–10.
[23] F. Ziegler, H. Irschik, R. Heuer, Response of polygonally shaped membranes to random excitation, in: I. Elishakoff, R.H. Lyon (Eds.), Random Vibration-Status and Recent Developments, Elsevier, Amsterdam, 1986, pp. 555–565.